NEOPLASIA
www.neoplasia.com
Volume 11 Number 6 June 2009 pp. 574–582 574

# A Comparison between Radiolabeled Fluorodeoxyglucose Uptake and Hyperpolarized $^{13}$C-Labeled Pyruvate Utilization as Methods for Detecting Tumor Response to Treatment[1,2]

**Timothy H. Witney*,†, Mikko I. Kettunen*,†, Samuel E. Day*,3, De-en Hu*,†, Andre A. Neves*,†, Ferdia A. Gallagher*,†,‡, Sandra M. Fulton* and Kevin M. Brindle*,†**

*Department of Biochemistry, University of Cambridge, Tennis Court Road, Cambridge CB2 1GA, United Kingdom; †Cancer Research UK Cambridge Research Institute, Li Ka Shing Centre, Robinson Way, Cambridge, CB2 0RE, United Kingdom; ‡Department of Radiology, University of Cambridge, Level 5, Box 219 Addenbrooke's Hospital, Hills Road, Cambridge CB2 2QQ, United Kingdom

## Abstract

Detection of early tumor responses to treatment can give an indication of clinical outcome. Positron emission tomography measurements of the uptake of the glucose analog, [$^{18}$F] 2-fluoro-2-deoxy-D-glucose (FDG), have demonstrated their potential for detecting early treatment response in the clinic. We have shown recently that $^{13}$C magnetic resonance spectroscopy and spectroscopic imaging measurements of the uptake and conversion of hyperpolarized [1-$^{13}$C]pyruvate into [1-$^{13}$C]lactate can be used to detect treatment response in a murine lymphoma model. The present study compares these magnetic resonance measurements with changes in FDG uptake after chemotherapy. A decrease in FDG uptake was found to precede the decrease in flux of hyperpolarized $^{13}$C label between pyruvate and lactate, both in tumor cells *in vitro* and in tumors *in vivo*. However, the magnitude of the decrease in FDG uptake and the decrease in pyruvate to lactate flux was comparable at 24 hours after drug treatment. In cells, the decrease in FDG uptake was shown to correlate with changes in plasma membrane expression of the facilitative glucose transporters, whereas the decrease in pyruvate to lactate flux could be explained by an increase in poly(ADP-ribose) polymerase activity and subsequent depletion of the NAD(H) pool. These results show that measurement of flux between pyruvate and lactate may be an alternative to FDG–positron emission tomography for imaging tumor treatment response in the clinic.

*Neoplasia (2009) 11, 574–582*

## Introduction

The introduction of new cancer therapies into the clinic, coupled with the highly variable responses of individual patients to these treatments, has stimulated the development of imaging methods that can give an early indication of treatment response [1,2]. These would allow the most appropriate therapy to be selected at an early stage during treatment, with consequent welfare benefits for the patient and cost benefits for the health-care system.

Abbreviations: 3-AB, 3-aminobenzamide; FDG, [$^{18}$F] 2-fluoro-2-deoxy-D-glucose; ID/g, injected dose per gram; MRSI, magnetic resonance spectroscopic imaging; 2-NBDG, 2-(*N*-(7-nitrobenz-2-oxa-1,3-diazol-4-yl)amino)-2-deoxyglucose; PARP, poly(ADP-ribose) polymerase; PET, positron emission tomography

Address all correspondence to: Prof. Kevin M. Brindle, Department of Biochemistry, University of Cambridge, Tennis Court Road, Cambridge CB2 1GA, United Kingdom.
E-mail: kmb1001@cam.ac.uk

[1]This work was supported by a Cancer Research UK Programme grant (to K.M.B.; C197/A3514). T.H.W. is in receipt of a GE Healthcare-BBSRC CASE studentship, S.E.D. a National Institutes of Health–Cambridge studentship, and F.A.G. a Cancer Research UK and Royal College of Radiologists (United Kingdom) clinical research training fellowship. S.M.F. is funded by Girton College, University of Cambridge. The polarizer and related materials were provided by GE Healthcare.
[2]This article refers to supplementary materials, which are designated by Figure W1 and Tables W1 and W2 and are available online at www.neoplasia.com.
[3]Current address: National Institute for Neurological Disorders and Stroke, National Institutes of Health, Bethesda, Maryland 20892-1065, USA.
Received 31 January 2009; Revised 16 March 2009; Accepted 17 March 2009


DOI 10.1593/neo.09254

Tumor responses to treatment are still largely assessed from measurements of changes in tumor size [2]. However, this approach lacks sensitivity because in many cases several weeks may elapse before there is evidence of tumor shrinkage. An observable change in tumor size might also not be detected despite a positive response to treatment, e.g., after cytostatic therapy. Recent advances in our understanding of tumor biology have resulted in the development of molecular-based approaches for detecting response to therapy using targeted noninvasive imaging methods [1–3].

Many tumors exhibit significantly increased glucose utilization in comparison to normal tissue (the "Warburg effect"), which is thought to be due largely to an increase in the expression and plasma membrane presentation of the facilitative glucose transporters, primarily the isoforms GLUT-1 and GLUT-3 [4]. In addition, there is increased expression of the glycolytic enzymes, accompanied by a shift in glucose metabolism from oxidative phosphorylation to glycolysis [5]. Increased glucose uptake and phosphorylation have been exploited clinically to detect tumors and their response to treatment using positron emission tomography (PET). [$^{18}$F] 2-Fluoro-2-deoxy-D-glucose (FDG), a glucose analog labeled with the positron-emitting isotope, $^{18}$F, is taken up by the cell through the GLUT transporters and is phosphorylated to FDG–6-phosphate by hexokinase. Further metabolism is blocked owing to the lack of a C-2 hydroxyl group, and FDG–6-phosphate becomes trapped within the cell. Increased uptake of FDG by tumor cells can thus be detected using PET [6]. Studies in lung [7], breast [8], esophageal [9], lymphoma [10], and ovarian cancers [11] have demonstrated that reduced FDG uptake can identify early treatment response. FDG-PET, however, is not effective in all tumor types because some tumors, e.g., prostate adenocarcinoma, show low FDG uptake [12], whereas in others, a high background uptake by surrounding normal tissue can mask tumor uptake, for example, in the brain [13] or in the presence of infected or inflamed tissue [14]. Furthermore, after treatment, high uptake by infiltrating immune cells can mask the decreased uptake by the dying tumor cells [15]. Quantitative analysis of tumor metabolic activity (known as standardized uptake value), can also pose problems and can be affected by a variety of different factors such as scanner resolution (making accurate estimation of FDG uptake in tumors smaller than 3 cm difficult) [16], partial volume effects caused by tumor heterogeneity [17], patient's glucose levels [18], and image acquisition and processing methods [19]. Thus, there is a need to develop alternative and complementary techniques for detecting tumor responses to treatment.

Dynamic nuclear polarization of $^{13}$C-labeled molecules can increase their sensitivity of detection in a solution-state nuclear magnetic resonance experiment by >10,000 times [20]. This dramatic increase in sensitivity means that, after intravenous injection, the spatial distribution of the labeled molecule and its subsequent metabolism can be imaged *in vivo* using $^{13}$C magnetic resonance spectroscopic imaging (MRSI) techniques. We have shown recently that the response of a murine lymphoma to drug treatment can be monitored by measuring the decrease in label flux between hyperpolarized [1-$^{13}$C]pyruvate and lactate in the reaction catalyzed by lactate dehydrogenase (LDH) [21]. The decrease in flux is likely to be due to a number of factors, including loss of enzyme from the cell, a decrease in tumor cellularity, and decreases in tumor lactate and NAD(H) concentrations. Because it has been proposed that this technique could be translated into the clinic for response monitoring [21], it is important to compare it with a molecular imaging technique that is used currently for this purpose in the clinic, FDG-PET. In this study, we compare changes in both FDG uptake and flux of hyperpolarized $^{13}$C label between pyruvate and lactate in mouse lymphoma cells *in vitro* and in implanted lymphoma tumors *in vivo* after drug-induced cell death.

## Materials and Methods

### *Materials*

Tissue culture reagents, 2-(*N*-(7-nitrobenz-2-oxa-1,3-diazol-4-yl) amino)-2-deoxyglucose (2-NBDG), SYTOX Red dead cell stain and annexin V–Pacific Blue were from Invitrogen (Paisley, Refrewshire, United Kingdom). All chemicals were of analytical grade from Sigma-Aldrich, Co., Ltd. (Poole, Dorset, United Kingdom). Etoposide (EPOSIN) was from PCH Pharmachemie (Haarlem, the Netherlands). 2-Fluoro-2-deoxy-D-[U-$^{14}$C]glucose was and [$^{14}$C]3-*O*-methylglucose were from American Radiolabeled Chemicals, Inc. (St. Louis, MO), and the poly(ADP-ribose) polymerase (PARP) assay kit was from R&D Systems (Minneapolis, MN). Murine lymphoma (EL-4) cells were from the European Collection of Cell Cultures (Salisbury, Wiltshire, United Kingdom).

### *Cell Culture*

EL-4 cells were grown in RPMI 1640 medium, supplemented with 10% fetal calf serum, 2 mM L-glutamine, 100 units/ml penicillin, and 100 μg/ml streptomycin. Cell number and viability were monitored using trypan blue staining. Cell death was induced by the addition of etoposide (final concentration, 15 μM).

### *Detection of Cell Death* In Vitro

Apoptosis and necrosis were visualized by staining with acridine orange (5 μg/ml) and propidium iodide (25 μg/ml) [22]. For measurements of cell death by flow cytometry, cell pellets ($1 \times 10^6$ cells) were washed in ice-cold HEPES-buffered saline (10 mM HEPES, 140 mM NaCl, 2.5 mM $CaCl_2$, pH 7.4) and resuspended in 100 μl of the same buffer. Annexin V–Pacific Blue was added (5 μl/100 μl of cell suspension) in combination with SYTOX Red (5 nM), before incubating for 10 minutes at 20°C. The resulting mixture was washed once, kept briefly on ice, and then analyzed in an LSRII Cytometer (BD Biosciences, Rockville, MD), with 20,000 cells counted per event. Residual cell debris, identified on forward (FS) and side light scattering (SS) profiles, was excluded from the analysis by selective gating. Cell death was also detected in the presence of the PARP inhibitor 3-aminobenzamide (3-AB; 10 mM).

### *Cell Uptake of [$^{14}$C]FDG and 2-NBDG*

[$^{14}$C]FDG (7.4 kBq; specific radioactivity, 11.1 GBq/mmol; radioactive concentration, 3.75 MBq/ml; radiochemical purity, 99%) was added to cells ($2 \times 10^6$) and incubated for 60 minutes at 37°C. Cells were collected by centrifugation (1300*g* for 3 minutes), washed twice with ice-cold PBS, and lysed in 0.2% SDS. FDG uptake was quantified by scintillation counting using an LS 6500 liquid scintillation counter (Beckman Coulter, Inc., Fullerton, CA). Uptake of 2-NBDG was measured by flow cytometry. After etoposide treatment, cells ($1 \times 10^6$) were incubated for 60 minutes at 37°C in a growth medium containing 2-NBDG (100 μM), washed twice with ice-cold HEPES-buffered saline, and then analyzed in an LSRII Cytometer (BD Biosciences), with 20,000 cells counted per event.

### *Poly(ADP-Ribose) Polymerase Activity Assay*

Cells ($2 \times 10^7$) were treated with etoposide, washed and then extracted using 1× Passive Lysis Buffer (Promega UK, Ltd., Southampton, Hampshire, United Kingdom) with Complete MINI EDTA-free protease inhibitor cocktail (Roche Applied Science, Mannheim, Germany) for 30 minutes at 4°C. Poly(ADP-ribose) polymerase activity in the resulting lysates was determined using the PARP Universal Colorimetric Assay according to the manufacturer's instructions. Protein content was determined using Bradford's reagent (Bio-Rad, Hercules, CA), and specific PARP activity was expressed as activity per milligram of total protein. One unit of PARP incorporates 100 pmol of poly(ADP-ribose) from $NAD^+$ into acid-insoluble form in 1 minute at 22°C.

### *Hexokinase Activity Assay*

Hexokinase activity was determined as described in Bergmeyer et al. [23]. The assay medium contained 39 mM triethanolamine, 216 mM D-glucose, 0.74 mM ATP, 7.8 mM magnesium chloride, 1.1 mM β-$NADP^+$, 2.5 U of glucose-6-phosphate dehydrogenase, pH 7.6. The assay was initiated by addition of 30 μl of a whole-cell lysate (prepared as in the PARP activity assay), and the reaction was followed spectrophotometrically at 340 nm. One unit of hexokinase activity is defined as the amount of enzyme that will phosphorylate 1.0 μmol of D-glucose/min at 25°C.

### *Western Blots*

Poly(ADP-ribose) polymerase cleavage and plasma membrane and total expression of the glucose transporter isoforms, GLUT-1 and GLUT-3, were assessed by Western blot analysis. Plasma membrane proteins were fractionated using a kit from Biovision (Mountain View, CA). The final protein pellet was resuspended in 0.5% SDS in PBS. For whole-cell lysate preparation, cells were washed twice in ice-cold PBS, solubilized in modified RIPA lysis buffer (50 mM Tris pH 7.8, 150 mM NaCl, 5 mM EDTA, 15 mM $MgCl_2$, 1% NP-40, 0.5% sodium deoxycholate, 1 mM 1,4-dithioerythritol, 20 mM *N*-ethylmaleimide), and passed five times through a 26G needle. Cell debris was removed by centrifugation (16,100*g*, 5 minutes, 4°C). Protein concentrations were determined using Bradford's reagent (Bio-Rad). A Non-Interfering Protein Assay kit (Merck Chemicals, Ltd., Darmstadt, Germany) was used to determine protein concentrations in the purified plasma membrane fractions.

Proteins were resolved by SDS-PAGE on a 10% gel and transferred on to polyvinylidene fluoride membranes (10 V, 30 minutes). Membranes were probed using polyclonal rabbit anti–GLUT-1 (1:2500; Abcam, Cambridge, Cambridgeshire, United Kingdom), polyclonal goat anti–GLUT-3 antibodies (1:1000; Santa Cruz Biotechnology, Inc., Santa Cruz, CA), and polyclonal rabbit anti-PARP1 (1:1000; Abcam). Antibodies for rabbit anti-HSP70 (1:2000; kindly provided by Dr. Haley Whitaker) and rabbit antiactin (1:1000; Sigma-Aldrich, Co., Ltd.) were used as loading controls. Peroxidase-conjugated donkey anti–rabbit IgG (1:10,000; Jackson ImmunoResearch Europe, Ltd., Newmarket, United Kingdom) and peroxidase-conjugated rabbit anti–goat IgG (1:4000; DarkoCytomation, Denmark) were used as secondary antibodies. Proteins were visualized using the ECLplus kit (GE Healthcare, Chalfont St Giles, Bucks, United Kingdom). Blots were scanned (PowerLook III; Umax Systems GmbH, Willich, Germany), and quantitation of the GLUT-3 signals was performed by densitometry using a scanning analysis software (TotalLab TL120; Nonlinear Dynamics, Newcastle upon Tyne, United Kingdom).

### *[1-$^{13}$C]Pyruvate Hyperpolarization*

A 44-mg sample of 91% [1-$^{13}$C]pyruvic acid containing 15 mM trityl radical OXO63 (GE Healthcare, Little Chalfont, United Kingdom) was hyperpolarized as described previously [20,21]. The frozen sample was dissolved at 180°C in 6 ml of buffer containing 40 mM HEPES, 94 mM NaOH, 30 mM NaCl, 50 mg/L EDTA, pH 12.5. The sample was dissolved in less than 10 seconds, and polarization levels were between 18% and 25%.

### *Nuclear Magnetic Resonance Spectroscopy of Cells*

Cells ($1 \times 10^8$) in RPMI 1640 medium were examined in a 10-mm nuclear magnetic resonance tube, using a broadband probe (Varian NMR Instruments, Palo, Alto, CA) in a 9.4-T vertical wide-bore magnet (Oxford Instruments, Abingdon, Oxfordshire, United Kingdom). The sample temperature was maintained at 37°C. Hyperpolarized [1-$^{13}$C]pyruvate (75 mM) and nonhyperpolarized, unlabeled lactate (75 mM) were injected into the cell suspension, and single-transient $^{13}$C spectra were acquired every second for 400 seconds, using a 6° flip angle pulse and a spectral width of 32 kHz.

### *Tumor Implantation*

Female C57BL/6 mice (Charles River, Ltd., Wilmington, MA), at an age of 6 to 8 weeks, were injected subcutaneously (in the lower flank) with $5 \times 10^6$ EL-4 cells, and the tumors were allowed to grow for 10 days (volume, ~2 $cm^3$) [24]. Mice were treated with an intraperitoneal injection of 67 mg of etoposide/kg body weight. All procedures were carried out in accordance with the Animals (Scientific Procedures) Act of 1986 (UK) and were designed with reference to the UK Coordinating Committee on Cancer Research Guidelines for the Welfare of Animals in Experimental Neoplasia. Tumor cell death was assessed histologically, using the National Institutes of Health ImageJ program to estimate the fraction occupied by the fragmented nuclei of dead cells in a 1.2-$mm^2$ field of view in tumor sections stained with hematoxylin and eosin [24]. Tumor size was reported as the product of the two largest perpendicular diameters ($mm^2$).

### *Tumor Uptake of [$^{14}$C]FDG*

Mice were anesthetized with an intraperitoneal injection of 10 ml/kg body weight of a 5:4:31 mixture of Hypnorm (VetaPharma, Ltd., Leeds, West Yorkshire, United Kingdom), Hypnovel (Roche, Basel, Switzerland), and saline and were injected intravenously with 14.8 kBq of [$^{14}$C]FDG in sterile saline. Tumor FDG uptake was measured at 60 minutes after injection. Mice were euthanized by cervical dislocation, and the tumors were excised and homogenized in RIPA buffer (150 mM NaCl, 1.0% Igepal CA-630, 0.5% sodium deoxycholate, 0.1% SDS, 50 mM Tris, 1 mM EDTA, pH 8.0; 10 ml of buffer/g of tumor tissue) using a General Laboratory Homogenizer (OMNI International, Warrenton, VA) and incubated at 24°C for 30 minutes. Cell debris was removed by centrifuging at 3000*g* for 10 minutes. The resulting supernatant was retained, and [$^{14}$C]FDG uptake was quantified by liquid scintillation counting.

### *Nuclear Magnetic Resonance Spectroscopy of Tumors*

Mice were anesthetized, and a catheter was inserted into a tail vein. A 25-mm-diameter surface coil tuned to $^{13}C$ (100 MHz) was positioned over the tumor. The entire assembly was placed in a quadrature $^{1}H$-tuned volume coil (Varian), in a 9.4-T vertical wide-bore magnet. Transverse $^{1}H$ images were acquired from the tumor using a spin-echo pulse sequence (repetition time, 1.5 seconds; echo time, 30 milliseconds; field of view, 32 mm × 32 mm; data matrix, 256 × 256; slice thickness, 2 mm; 11 slices). After injection of hyperpolarized [1-$^{13}C$]pyruvate, which was accomplished within 3 seconds, 128 single-transient spectra were collected from a 5-mm-thick tumor slice for a period of 128 seconds (every 16th spectrum was collected from the entire sensitive volume of the surface coil). Spectra were acquired using a slice-selective 600-microsecond sinc pulse, with a nominal flip angle of 5°.

### *Estimation of Hyperpolarized $^{13}C$ Label Flux between Pyruvate and Lactate*

The peak intensities of hyperpolarized [1-$^{13}C$]lactate and [1-$^{13}C$]pyruvate were fitted to the modified Bloch equations for a two-site exchange to obtain a rate constant for flux of label between pyruvate and lactate ($k_P$). The limitations of this model for estimating flux have been discussed previously [21].

### *Statistics*

Results are expressed as the mean ± SEM. Significant differences between mean values were determined by analysis of variance (ANOVA) followed by Dunnett's *post hoc* test. Differences between treatment groups were considered significant if $P < .05$.

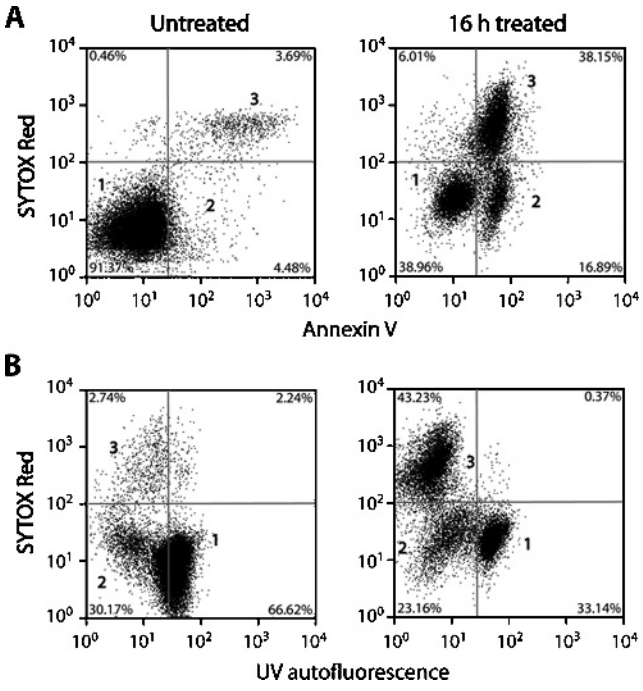


**Figure 1.** Flow cytometric analysis of EL-4 cells treated for 16 hours with etoposide. (A) Detection of apoptotic cells using annexin V—Pacific Blue ($\lambda$ Ex/Em = 410/455) and necrotic cells by SYTOX Red nuclear staining ($\lambda$ Ex/Em = 640/658). (B) Changes in cellular autofluorescence after treatment. The autofluorescence observed at 455 nm with excitation at 350 nm has been assigned to NADH [25,26]. Population 1 represents viable cells, whereas population 2 represents apoptotic cells that have a low UV autofluorescence and stain with annexin V. Population 3 represents necrotic cells.

## Results

### *Measurement of Cell Death* In Vitro

Cell death was analyzed by flow cytometry of cells that had been stained with annexin V–Pacific Blue, which labels apoptotic and necrotic cells, and SYTOX Red dead cell stain, which labels necrotic cells (Figure 1). The onset of apoptosis was detectable at 8 hours after treatment (77% ± 8% increase in median fluorescence, $n = 4$, $P < .01$), rising to a maximum at 16 hours (920% ± 130% increase; Figure 2*A*). The necrotic cell fraction remained largely unchanged throughout the treatment time course, with a significant increase in necrosis becoming detectable at 16 hours ($P < .05$). Similar results were obtained by fluorescence microscopy of cells stained with acridine orange and propidium iodide (data not shown).

### *Measurements of Hyperpolarized [$^{13}C$] Label Flux between Pyruvate and Lactate in Cells*

Addition of hyperpolarized [1-$^{13}C$]pyruvate to cells resulted in an increase in the lactate carboxyl signal intensity, because the label was transferred from pyruvate, followed by a decrease in signal intensity due to decay of the polarization (Figure 3). Changes in the rate constant describing the flux between [1-$^{13}C$]pyruvate and [1-$^{13}C$]lactate ($k_P$) were observed in cells after the induction of apoptosis by etoposide treatment. A 23% decrease was detected at 12 hours after treatment, although the decrease in the rate did not reach statistical significance until 14 hours ($P < .01$). By 16 hours, the rate constant had fallen from $3.6 \times 10^{-4} \pm 0.6 \times 10^{-4}$ s$^{-1}$ to $0.6 \times 10^{-4} \pm 0.1 \times 10^{-4}$ s$^{-1}$, a decrease of 83% ($P < .01$; Figure 2*B*, *right axis*). The fitted values for the rate constant $k_P$, the values for the rate constant describing flux between [1-$^{13}C$]lactate and [1-$^{13}C$]pyruvate ($k_L$), and the apparent spin lattice relaxation rates for [1-$^{13}C$]lactate ($\rho_L$) and [1-$^{13}C$]pyruvate ($\rho_P$), which were assumed to be equal, are shown in Table W1.

The decreased pyruvate–lactate flux in etoposide-treated EL-4 cells has been shown previously to be due predominantly to PARP-mediated depletion of the NAD(H) pool [21] because inhibition of PARP largely prevented the decrease in the rate constant $k_P$. We have demonstrated here a temporal correlation between PARP-mediated depletion of NAD(H) and the loss of flux between pyruvate and lactate in drug-treated cells (Figures 1*B* and 2*C*). NAD(H) depletion was assessed from the loss of cellular UV autofluorescence (excitation at 350 nm; emission at 475 nm). Cytoplasmic NADH has been shown previously to make a significant contribution to this autofluoresence [25], and it is the cytosolic, rather than the mitochondrial NAD(H) pool, that is depleted after PARP activation [26]. There was a significant decrease in autofluorescence by 10 hours after drug treatment (58% decrease, $P < .01$), a time at which there had been a significant increase in PARP activity (238% increase, $P < .05$). Poly(ADP-ribose) polymerase activity rose to a peak at 14 hours after treatment, which was five-fold greater than that of the control, untreated cells. Cellular autofluorescence declined to a minimum at 12 hours. Addition of a PARP inhibitor, 3-AB, inhibited loss of cellular UV autofluorescence after drug treatment, confirming that the UV autofluorescence correlates with the cytosolic

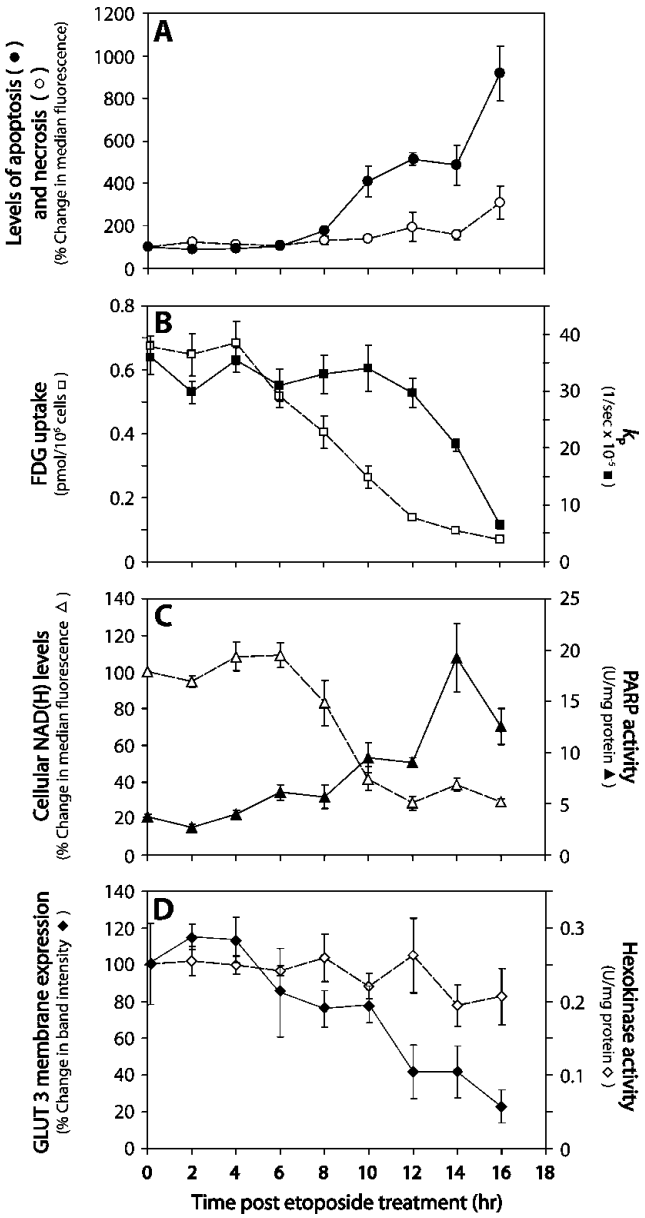


**Figure 2.** Changes in cell metabolism after etoposide-induced apoptosis of EL-4 cells. (A) Apoptosis (●) and necrosis (○) determined by flow cytometry. Apoptotic cells were detected using annexin V–Pacific Blue ($\lambda$ Ex/Em = 410/455) and necrotic cells using SYTOX Red nuclear staining ($\lambda$ Ex/Em = 640/658). (B) Changes in [1-$^{13}$C]pyruvate to [1-$^{13}$C]lactate flux (■) and [$^{14}$C]FDG uptake (□) after etoposide treatment. The rate constants for label flux from pyruvate to lactate ($k_P$) were derived by fitting changes in signal peak intensity to the modified Bloch equations for two-site exchange [21]. Cell number–corrected uptake of [$^{14}$C]FDG was measured in cells at 60 minutes after adding the radiotracer. (C) Changes in cellular autofluorescence (△) and PARP activity (▲) in etoposide-treated cells. UV autofluorescence was detected by flow cytometry ($\lambda$ Ex/Em = 350/455), and PARP activity by ELISA. (D) Hexokinase activity (◇) and GLUT-3 plasma membrane expression (◆) in treated EL-4 cells. Hexokinase activity in cell lysates was determined by measuring the reduction of $NADP^+$ in a coupled reaction with glucose-6-phosphate dehydrogenase, as described in Bergmeyer et al. [23]. GLUT-3 levels in plasma membrane protein fractions were assessed by Western blot. Quantitation of bands was determined by densitometry and expressed as a percentage of GLUT-3 expression in untreated cells. Data shown as mean ± SEM ($n$ = 3-5).

NADH concentration. The median fluorescence of cells treated with etoposide and 3-AB for 16 hours was 92% ± 14% ($n$ = 4) of the untreated control cells.

Caspase 3–mediated cleavage of PARP was evaluated by Western blot analysis of whole-cell lysates (Figure 4). The cleaved 25-kDa PARP fragment was detected 6 hours after treatment after prolonged exposure of the blot, with levels of cleaved PARP increasing throughout the remainder of the time course.

### *FDG Uptake in Cells*

Uptake of FDG was measured during a period of 16 hours after etoposide treatment (Figure 2*B*, *left axis*). [$^{14}$C]FDG was added to treated cells, and its intracellular accumulation was measured after 60 minutes. A 22% reduction in uptake (adjusted for cell number) was observed at 6 hours after drug treatment, falling from 6.7 ± 0.3 pmol/$10^7$ cells in untreated cells to 5.2 ± 0.4 pmol/$10^7$ in treated cells ($n$ = 9, $P$ < .01). The uptake rate dropped steadily during the following 10 hours, to 10% of the FDG uptake rate in untreated cells by 16 hours (0.7 ± 0.05 pmol/$10^7$ cells). The uptake of a fluorescent glucose analog, 2-NBDG [27], was also evaluated by flow cytometry. This showed a similar profile to FDG of reduced uptake as a function of time (Figure W1).

To test whether changes in FDG uptake were a result of changes in the transport rate or subsequent phosphorylation, both hexokinase activity and glucose transporter expression were measured as a function of time after etoposide treatment (Figure 2*D*). There was no significant change in extractable hexokinase activity during the 16 hours after drug treatment. Treatment with etoposide resulted in minimal changes in both GLUT-1 and GLUT-3 expression in whole-cell lysates during 16 hours after drug treatment (Figure 5*A*); however, there was a decrease in GLUT-1 and GLUT-3 levels in the plasma membrane fraction at 6 hours, which further decreased throughout the remainder of the treatment time course, closely paralleling the pattern of reduced FDG uptake after treatment (Figures 2*D* and 5*B*). These results suggest that etoposide treatment causes the glucose transporters to translocate from the plasma membrane to the cytosol, resulting in a decrease in FDG uptake.

### *Monitoring Treatment Response in Tumors*

Intravenous injection of hyperpolarized [1-$^{13}$C]pyruvate (0.2 ml, 75 mM) into EL-4 tumor-bearing mice resulted in the appearance of signals from [1-$^{13}$C]pyruvate and [1-$^{13}$C]lactate in the tumors (Figure 3). Treatment with etoposide for 16 and 24 hours resulted in 15% ± 2% and 31% ± 4% cell death, respectively, in comparison to 4% ± 1% in untreated tumors ($n$ = 3), as assessed by histological analysis of tumor sections obtained *postmortem*. Drug treatment resulted in a reduction in tumor volume from 282 ± 16 to 251 ± 15 mm$^2$ at 16 hours after treatment (11% decrease, $P$ > .05, $n$ = 5), decreasing further to 199 cm ± 13 mm$^2$ at 24 hours after treatment (30% decrease, $P$ < .01, $n$ = 5). There was no significant change in flux between pyruvate and lactate at 16 hours after treatment ($n$ = 5 animals), but by 24 hours, there was a 38% decrease in the rate constant $k_P$ from 0.056 ± 0.005 s$^{-1}$ ($n$ = 5 animals) to 0.034 ± 0.006 s$^{-1}$ ($P$ < .05, $n$ = 6 animals; Figure 6*A*). The fitted values for the rate constants $k_L$ and $k_P$ and the apparent spin lattice relaxation rates ($\rho_L$ and $\rho_P$) are shown in Table W2.

[$^{14}$C]FDG uptake was measured in tumors after drug treatment (Figure 6*B*). Measurements of FDG uptake in excised tissue show good agreement with PET measurements of FDG uptake [28]. There was a

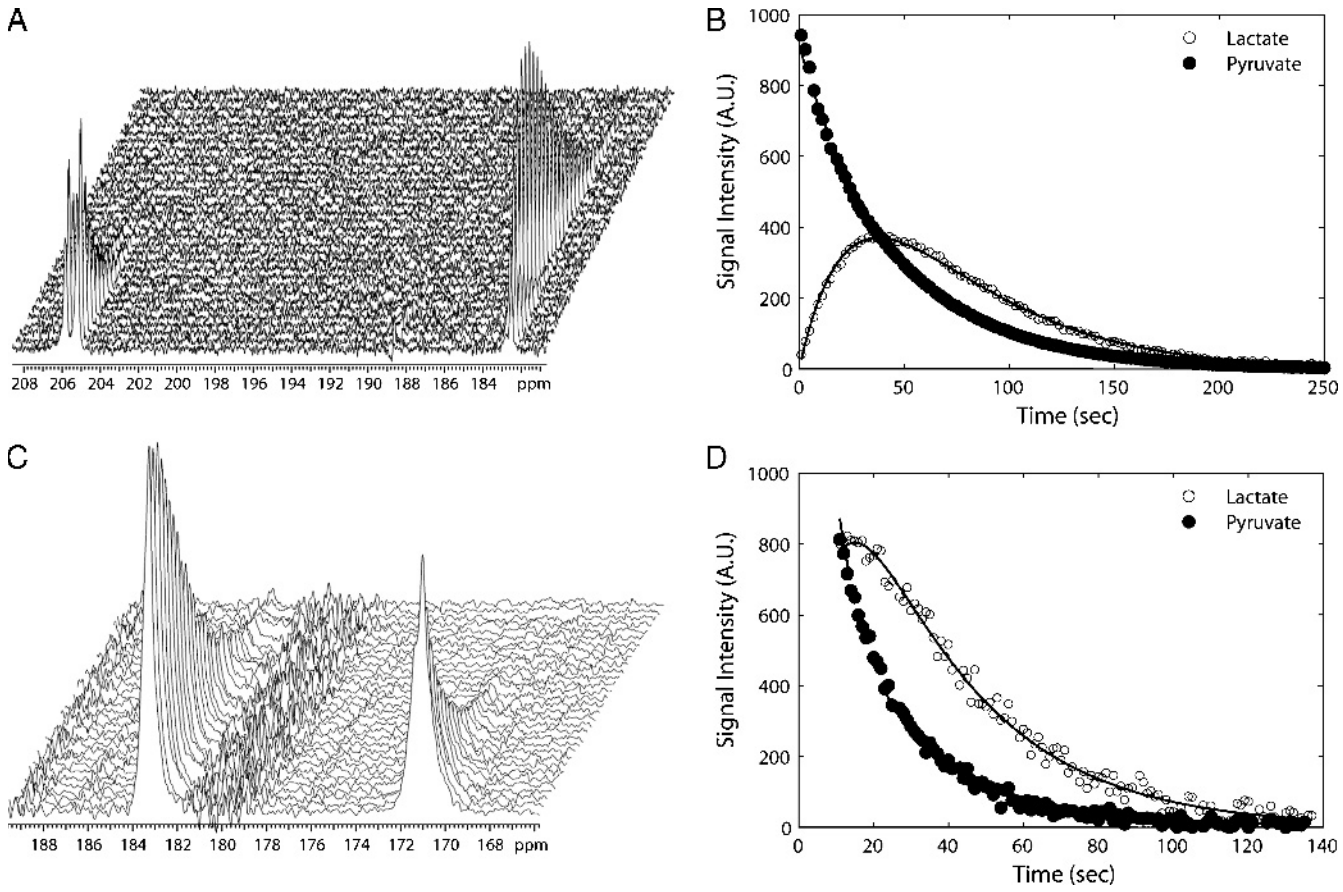


**Figure 3.** Measurements of hyperpolarized $^{13}C$ label flux between pyruvate and lactate in cells and in tumors. Sequential $^{13}C$ spectra from cells (A) and a tumor (C), showing signals from hyperpolarized [1-$^{13}C$]pyruvate (at 171 ppm) and [1-$^{13}C$]lactate (at 183 ppm). The peaks at 206 ppm in (A) are from natural abundance [2-$^{13}C$]pyruvate. Example of fits of the [1-$^{13}C$]pyruvate and [1-$^{13}C$]lactate peak intensities from the cell (B) and tumor spectra (D) to a two-site exchange model [21]. Fits are shown as solid lines. The pyruvate peak intensity was divided by 100 in (B). For clarity, only every fourth data point is shown. AU indicates arbitrary units.

16% decrease in FDG uptake at 16 hours after treatment, falling from 12.7% ± 0.6% injected dose per gram of tissue (ID/g) to 10.6% ± 0.6% ID/g ($P < .05$, $n = 6$ animals). At 24 hours, FDG uptake was 7.9% ± 0.6% ID/g ($P < .001$, $n = 12$ animals), 38% lower than the pretreatment uptake value ($n = 11$ animals).

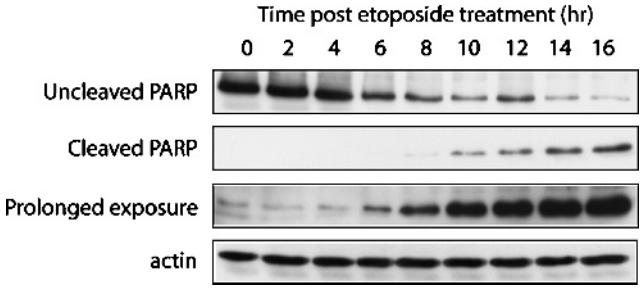


**Figure 4.** Caspase 3–mediated PARP cleavage after etoposide treatment. Western blot analysis of the levels of uncleaved (113 kDa) and cleaved PARP (25 kDa) in whole-cell lysates of etoposide-treated cells during a 16-hour time course. The blot was also subjected to a prolonged exposure to identify the onset of caspase 3–mediated PARP cleavage. Actin was used as a loading control.

## Discussion

There is a pressing need to develop noninvasive imaging techniques for monitoring tumor treatment response in the clinic. FDG-PET has been shown to be a good predictive indicator of treatment response in a variety of different human cancers [7–11]; however, this technique has low sensitivity in slowly growing tumors with low metabolic activity (such as prostate adenocarcinoma) and measurements of tumor uptake may be difficult when surrounding normal tissue has high glucose metabolism (e.g., in the brain) [12,13]. We have recently reported an alternative method for detecting treatment response, which measures the decrease in the rate of LDH-catalyzed flux of hyperpolarized $^{13}C$ label between pyruvate and lactate using MRSI [21]. In this study, we compared the temporal changes in FDG uptake with those of hyperpolarized $^{13}C$ label flux between pyruvate and lactate in a murine lymphoma model after drug treatment.

Treatment with the topoisomerase type II inhibitor, etoposide, resulted in the induction of apoptosis in EL-4 cells *in vitro*. A reduction in FDG uptake was detected 6 hours after treatment, which occurred 2 hours before the exposure of the phospholipid, phosphatidylserine, and consequent binding of annexin V. This reduction in FDG uptake correlated with the translocation of both GLUT-1 and GLUT-3 transporters from the plasma membrane to the cytosol, as shown by Western blots of the whole cell and plasma membrane fractions. There were no

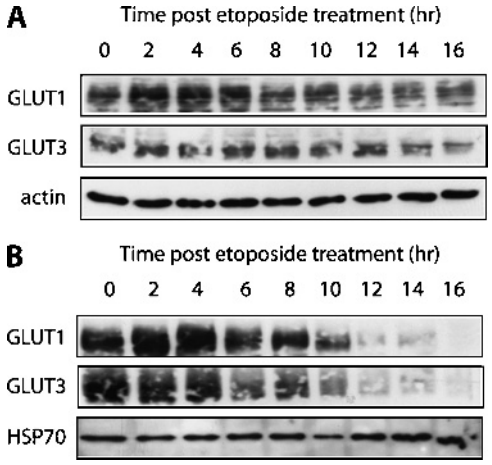


**Figure 5.** Effect of etoposide on glucose transporter membrane expression. Western blot analysis of GLUT-1 and GLUT-3 levels in whole-cell lysate (A) and plasma membrane protein fractions (B) of etoposide-treated cells during a 16-hour time course after drug treatment. HSP70 and actin were used as loading controls.

changes in the whole-cell levels of GLUT-1 or GLUT-3 or in the activity of hexokinase during the 16-hour time course. Previous studies in non–small cell lung cancer cells *in vitro* have shown that changes in plasma membrane glucose transporter expression can explain a reduction in FDG uptake after inhibition of epidermal growth factor receptor kinase [29]. Inhibition of epidermal growth factor receptor kinase results in inhibition of Akt (PKB) activity, which is known to enhance and maintain glucose transporter presentation on the plasma membrane [30]. The decrease in the plasma membrane presentation of GLUT-1 and GLUT-3 observed here might also be due to a decrease in Akt activity because Akt is known to be a substrate for caspases [31], and caspase-cleaved PARP first became evident at 6 hours after drug treatment (Figure 4) when there was also a decrease in GLUT-3 expression at the plasma membrane and a corresponding decrease in FDG uptake (Figure 2). The results obtained here, however, are in contrast to those obtained in pro–B-lymphocytic cells, where, after exposure to a range of genotoxic agents, including etoposide, a decrease in GLUT-1 and GLUT-3 expression was observed [32].

In contrast to the relatively early reduction in FDG uptake rate, the decrease in LDH-catalyzed flux of hyperpolarized $^{13}C$ label between pyruvate and lactate was not significant until 14 hours after drug treatment. We have shown previously that the decrease in label flux between pyruvate and lactate in EL-4 lymphoma cells *in vitro* could be explained predominantly by PARP-mediated depletion of the NAD(H) coenzyme pool because PARP inhibitors prevented the decrease in NAD(H) concentration, as determined from $^{31}P$ MRSI measurements on cells extracts, and also largely prevented the decrease in flux at 16 hours after drug treatment [21]. We have shown here a temporal correlation between measured PARP activity and a decrease in cellular UV autofluorescence, which is representative of the cytoplasmic NADH concentration [25,26]. There was a gradual increase in PARP activity after etoposide treatment, rising rapidly at 10 hours after treatment, by which time there was a significant decrease in cellular autofluorescence. Although the decrease in autofluorescence preceded the decrease in flux between pyruvate and lactate, this may reflect the $K_m$ of the enzyme for NAD(H), the enzyme being saturated with the coenzymes in untreated cells. The decrease in flux between pyruvate and lactate may be delayed by caspase 3–mediated cleavage of PARP (Figure 4), which is known to result in PARP inactivation [33]. In summary, in cells, the observed decrease in flux between pyruvate and lactate is associated with an increase in PARP activity and a subsequent decrease in the cellular NAD(H) pool.

The temporal changes in FDG uptake and hyperpolarized $^{13}C$ label flux were also evaluated in EL-4 tumors that had been produced by subcutaneous implantation of EL-4 cells. We had demonstrated previously, by measurements at a single time point, that hyperpolarized $^{13}C$ label flux between pyruvate and lactate was decreased at 24 hours after drug treatment and had shown that this was likely to be due to a number of factors, including a decrease in tumor lactate concentration, a reduction in tumor cellularity, and a loss of the enzyme from the cells as well as the coenzyme NAD(H) [21].

In the current study, we have shown that a significant decrease in FDG uptake was detectable at 16 hours after etoposide treatment, but the decrease in flux between pyruvate and lactate did not reach statistical significance until 24 hours after treatment when a significant decrease in tumor volume was observed. Therefore, both in isolated cells and in tumors *in vivo*, the decrease in FDG uptake preceded the decrease in flux of $^{13}C$ label between pyruvate and lactate in this lymphoma tumor model.

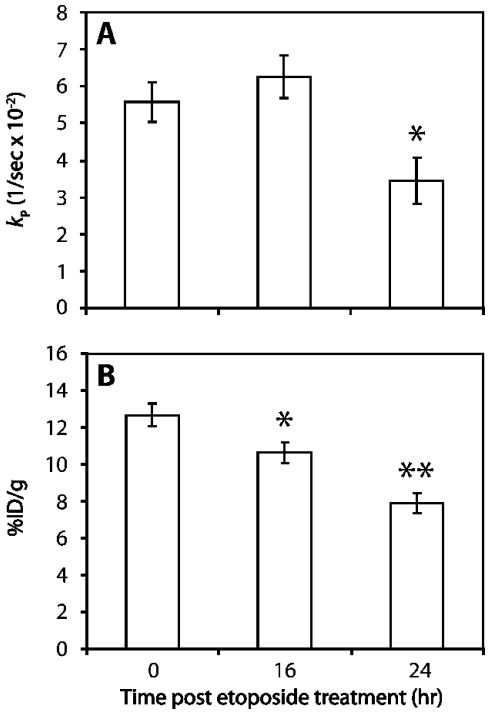


**Figure 6.** Comparison of [$^{14}C$]FDG uptake with hyperpolarized $^{13}C$ label flux between pyruvate and lactate in EL-4 tumors. (A) Changes in [1-$^{13}C$]pyruvate to [1-$^{13}C$]lactate flux in untreated EL-4 tumors and tumors treated with etoposide for either 16 or 24 hours. Changes in tumor pyruvate and lactate peak intensities were fitted to a two-site exchange model to obtain the rate constant for pyruvate to lactate flux. (B) Uptake of [$^{14}C$]FDG in untreated EL-4 tumors and tumors treated with etoposide for either 16 or 24 hours. [$^{14}C$]FDG was injected intravenously, and uptake was allowed to proceed for 60 minutes. Tumors were then excised and homogenized. Percentage injected dose per gram of tissue (%ID/g) was determined by liquid scintillation counting. Mean values ($n$ = 6-12) and SEs are shown (*$P < .05$, **$P < .01$).

A reduction in FDG uptake has been measured in the clinic as early as 24 hours after the first dose of chemotherapy, with the early PET response able to predict the later response with PET at day 8 in all patients [34]. These results, coupled with the results found in this study, indicate that some benefit may be derived from monitoring treatment response with FDG-PET at an early stage after treatment. However, there are other studies in which FDG uptake was reduced for a period of 2 weeks before increasing again in patients that failed to respond to therapy [35]. Conversely, false-positive results have also been detected early after therapy, and these are thought to correlate with an influx of inflammatory cells [15]. It is now generally accepted that scans performed 5 to 6 weeks after therapy are more accurate at indicating response than early monitoring [36–38]. In this context, the earlier detection of response that we have seen here with FDG may have no advantage in the clinic over the later detection of response using hyperpolarized $^{13}$C-labeled pyruvate.

Although the timing of response to treatment may vary between FDG-PET and hyperpolarized $^{13}$C, the fractional decrease in flux between pyruvate and lactate is nearly identical to the decrease in FDG uptake. This suggests that the magnetic resonance experiment could be as sensitive as the PET experiment for detecting treatment response. Moreover, MRSI avoids the use of ionizing radiation. The most important advantage of the technique, however, may be in assessing response in cancers, e.g., tumors of the brain and prostate, where FDG-PET is ineffective in measuring treatment response. A recent study in a transgenic mouse model of prostate cancer showed that changes in pyruvate to lactate flux can be used to predict response to antiandrogen therapy. In responding tumors, a reduction in pyruvate to lactate flux correlated with a reduction in tumor volume and an increase in mean survival time after hormone deprivation, with an increase in flux and tumor volume observed in the nonresponders [39].

## Acknowledgments

The authors thank Haley Whitaker for the donation of the rabbit anti-HSP70 antibody and for technical assistance with plasma membrane Western blot studies and Israt Alam for comments on the manuscript.

## References

[1] Brindle K (2008). New approaches for imaging tumour responses to treatment. *Nat Rev Cancer* **8**, 1–14.

[2] Neves AA and Brindle KM (2006). Assessing responses to cancer therapy using molecular imaging. *Biochim Biophys Acta* **1766**, 242–261.

[3] Weissleder R and Pittet MJ (2008). Imaging in the era of molecular oncology. *Nature* **452**, 580–589.

[4] Merrall NW, Plevin R, and Gould GW (1993). Growth-factors, mitogens, oncogenes and the regulation of glucose transport. *Cell Signal* **5**, 667–675.

[5] Gatenby RA and Gillies RJ (2004). Why do cancers have high aerobic glycolysis? *Nat Rev Cancer* **4**, 891–899.

[6] Czernin J and Phelps ME (2002). Positron emission tomography scanning: current and future applications. *Annu Rev Med* **53**, 89–112.

[7] Weber WA, Petersen V, Schmidt B, Tyndale-Hines L, Link T, Peschel C, and Schwaiger M (2003). Positron emission tomography in non–small-cell lung cancer: prediction of response to chemotherapy by quantitative assessment of glucose use. *J Clin Oncol* **21**, 2651–2657.

[8] Schelling M, Avril N, Nahrig J, Kuhn W, Romer W, Sattler D, Werner M, Dose J, Janicke F, Graeff H, et al. (2000). Positron emission tomography using [F-18]fluorodeoxyglucose for monitoring primary chemotherapy in breast cancer. *J Clin Oncol* **18**, 1689–1695.

[9] Weber WA, Ott K, Becker K, Dittler HJ, Helmberger H, Avril NE, Meisetschlager G, Busch R, Siewert JR, Schwaiger M, et al. (2001). Prediction of response to preoperative chemotherapy in adenocarcinomas of the esophagogastric junction by metabolic imaging. *J Clin Oncol* **19**, 3058–3065.

[10] Spaepen K, Stroobants S, Dupont P, Van Steenweghen S, Thomas J, Vandenberghe P, Vanuytsel L, Bormans G, Balzarini J, De WolfPeeters C, et al. (2001). Prognostic value of positron emission tomography (PET) with fluorine-18 fluorodeoxyglucose ([F-18]FDG) after first-line chemotherapy in non–Hodgkin's lymphoma: is [F-18] FDG-PET a valid alternative to conventional diagnostic methods? *J Clin Oncol* **19**, 414–419.

[11] Avril N, Sassen S, Schmalfeldt B, Naehrig J, Rutke S, Weber WA, Werner M, Graeff H, Schwaiger M, and Kuhn W (2005). Prediction of response to neoadjuvant chemotherapy by sequential F-18-fluorodeoxyglucose positron emission tomography in patients with advanced-stage ovarian cancer. *J Clin Oncol* **23**, 7445–7453.

[12] Takahashi N, Inoue T, Lee J, Yamaguchi T, and Shizukuishi K (2007). The roles of PET and PET/CT in the diagnosis and management of prostate cancer. *Oncology* **72**, 226–233.

[13] Phelps ME and Mazziotta JC (1985). Positron emission tomography — human-brain function and biochemistry. *Science* **228**, 799–809.

[14] Zhuang HM, Pourdehnad M, Lambright ES, Yamamoto AJ, Lanuti M, Li PY, Mozley PD, Rossman MD, Albelda SM, and Alavi A (2001). Dual time point F-18-FDG PET imaging for differentiating malignant from inflammatory processes. *J Nucl Med* **42**, 1412–1417.

[15] Strauss LG (1996). Fluorine-18 deoxyglucose and false-positive results: a major problem in the diagnostics of oncological patients. *Eur J Nucl Med* **23**, 1409–1415.

[16] Weber WA (2005). Use of PET for monitoring cancer therapy and for predicting outcome. *J Nucl Med* **46**, 983–995.

[17] Stahl A, Ott K, Schwaiger M, and Weber WA (2004). Comparison of different SUV-based methods for monitoring cytotoxic therapy with FDG PET. *Eur J Nuc Med Mol Imag* **31**, 1471–1479.

[18] Diederichs CG, Staib L, Glatting G, Beger HG, and Reske SN (1998). FDG PET: elevated plasma glucose reduces both uptake and detection rate of pancreatic malignancies. *J Nucl Med* **39**, 1030–1033.

[19] Thie JA (2004). Understanding the standardized uptake value, its methods, and implications for usage. *J Nucl Med* **45**, 1431–1434.

[20] Ardenkjaer-Larsen JH, Fridlund B, Gram A, Hansson G, Hansson L, Lerche MH, Servin R, Thaning M, and Golman K (2003). Increase in signal-to-noise ratio of >10,000 times in liquid-state NMR. *Proc Natl Acad Sci USA* **100**, 10158–10163.

[21] Day SE, Kettunen MI, Gallagher FA, Hu D-E, Lerche M, Wolber J, Golman K, Ardenkjaer-Larsen JH, and Brindle KM (2007). Detecting tumor response to treatment using hyperpolarized $^{13}$C magnetic resonance imaging and spectroscopy. *Nat Med* **13**, 1382–1387.

[22] Darzynkiewicz Z, Bruno S, Delbino G, Gorczyca W, Hotz MA, Lassota P, and Traganos F (1992). Features of apoptotic cells measured by flow-cytometry. *Cytometry* **13**, 795–808.

[23] Bergmeyer HU, Grassl M, and Walter HE (1983). Hexokinase. In HU Bergmeyer (Ed.). *Methods of Enzymatic Analysis.* Weinheim-Deerfield Beach, FL-Basel: Verlag Chemie, pp. 222–223.

[24] Schmitz JE, Kettunen MI, Hu DE, and Brindle KM (2005). $^{1}$H MRS-visible lipids accumulate during apoptosis of lymphoma cells *in vitro* and *in vivo*. *Magn Reson Med* **54**, 43–50.

[25] Aubin JE (1979). Autofluorescence of viable cultured mammalian cells. *J Histochem* **27**, 36–43.

[26] Ying WH, Alano CC, Garnier P, and Swanson RA (2005). NAD(+) as a metabolic link between DNA damage and cell death. *J Neurosci Res* **79**, 216–223.

[27] Cheng Z, Levi J, Xiong ZM, Gheysens O, Keren S, Chen XY, and Gambhir SS (2006). Near-infrared fluorescent deoxyglucose analogue for tumor optical imaging in cell culture and living mice. *Bioconjug Chem* **17**, 662–669.

[28] van Waarde A, Shiba K, de Jong JR, Ishiwata K, Dierckx RA, and Elsinga PH (2007). Rapid reduction of sigma(1)-receptor binding and F-18-FDG uptake in rat gliomas after *in vivo* treatment with doxorubicin. *J Nucl Med* **48**, 1320–1326.

[29] Su H, Bodenstein C, Dumont RA, Seimbille Y, Dubinett S, Phelps ME, Herschman H, Czernin J, and Weber W (2006). Monitoring tumor glucose utilization by positron emission tomography for the prediction of treatment response to epidermal growth factor receptor kinase inhibitors. *Clin Cancer Res* **12**, 5659–5667.

[30] Wieman HL, Wofford JA, and Rathmell JC (2007). Cytokine stimulation promotes glucose uptake via phosphatidylinositol-3 kinase/Akt regulation of Glut1 activity and trafficking. *Mol Biol Cell* **18**, 1437–1446.

[31] Widmann C, Gibson S, and Johnson GL (1998). Caspase-dependent cleavage of signaling proteins during apoptosis—a turn-off mechanism for anti-apoptotic signals. *J Biol Chem* **273**, 7141–7147.

[32] Zhou R, Vander Heiden MG, and Rudin CM (2002). Genotoxic exposure is associated with alterations in glucose uptake and metabolism. *Cancer Res* **62**, 3515–3520.

[33] Kaufmann SH, Desnoyers S, Ottaviano Y, Davidson NE, and Poirier GG (1993). Specific proteolytic cleavage of poly(ADP-ribose) polymerase—an early marker of chemotherapy-induced apoptosis. *Cancer Res* **53**, 3976–3985.

[34] Stroobants S, Goeminne J, Seegers M, Dimitrijevic S, Dupont P, Nuyts J, Martens M, van den Borne B, Cole P, Sciot R, et al. (2003). (18)FDG-Positron emission tomography for the early prediction of response in advanced soft tissue sarcoma treated with imatinib mesylate (Glivec). *Eur J Cancer* **39**, 2012–2020.

[35] Cremerius U, Effert PJ, Adam G, Sabri O, Zimny M, Wagenknecht G, Jakse G, and Buell U (1998). FDG PET for detection and therapy control of metastatic germ cell tumor. *J Nucl Med* **39**, 815–822.

[36] Barrington SF and O'Doherty MJ (2003). Limitations of PET for imaging lymphoma. *Eur J Nuc Med Mol Imag* **30**, S117–S127.

[37] Findlay M, Young H, Cunningham D, Iveson A, Cronin B, Hickish T, Pratt B, Husband J, Flower M, and Ott R (1996). Noninvasive monitoring of tumor metabolism using fluorodeoxyglucose and positron emission tomography in colorectal cancer liver metastases: correlation with tumor response to fluorouracil. *J Clin Oncol* **14**, 700–708.

[38] Romer W, Hanauske AR, Ziegler S, Thodtmann R, Weber W, Fuchs C, Enne W, Herz M, Nerl C, Garbrecht M, et al. (1998). Positron emission tomography in non–Hodgkin's lymphoma: assessment of chemotherapy with fluorodeoxyglucose. *Blood* **91**, 4464–4471.

[39] Chen AP, Bok R, Zhang V, Xu D, Veeraraghavan S, Hurd RE, Nelson SJ, Kurhanewicz J, and Vigneron DB (2008). Serial hyperpolarized $^{13}$C 3D-MRSI following therapy in a mouse model of prostate cancer. *Proc Int Soc Magn Reson Med* **16**, 888.

**Table W1.** Fitted Rate Constants for Untreated and Etoposide-Treated Cells.

| | $k_L$ ($\times 10^{-3}$ $s^{-1}$) | $k_P$ ($\times 10^{-3}$ $s^{-1}$) | $\rho_L = \rho_P$ ($s^{-1}$) |
|---|---|---|---|
| Untreated ($n$ = 4) | 8 ± 1 | 0.36 ± 0.03 | 0.027 ± 0.001 |
| 2 h ($n$ = 5) | 20 ± 4 | 0.30 ± 0.02 | 0.026 ± 0.001 |
| 4 h ($n$ = 6) | 13 ± 2 | 0.35 ± 0.02 | 0.027 ± 0.000 |
| 6 h ($n$ = 6) | 21 ± 2* | 0.31 ± 0.03 | 0.024 ± 0.002 |
| 8 h ($n$ = 6) | 18 ± 2 | 0.33 ± 0.03 | 0.025 ± 0.001 |
| 10 h ($n$ = 5) | 18 ± 3 | 0.34 ± 0.04 | 0.025 ± 0.002 |
| 12 h ($n$ = 4) | 8 ± 1 | 0.30 ± 0.03 | 0.023 ± 0.002 |
| 14 h ($n$ = 4) | 7 ± 2 | 0.21 ± 0.01* | 0.024 ± 0.001 |
| 16 h ($n$ = 4) | 6 ± 2 | 0.06 ± 0.01† | 0.027 ± 0.001 |

Values are presented as mean ± SEM.
*$P$ < .05, ANOVA followed by Dunnett's *post hoc* test.
†$P$ < .01, ANOVA followed by Dunnett's *post hoc* test.

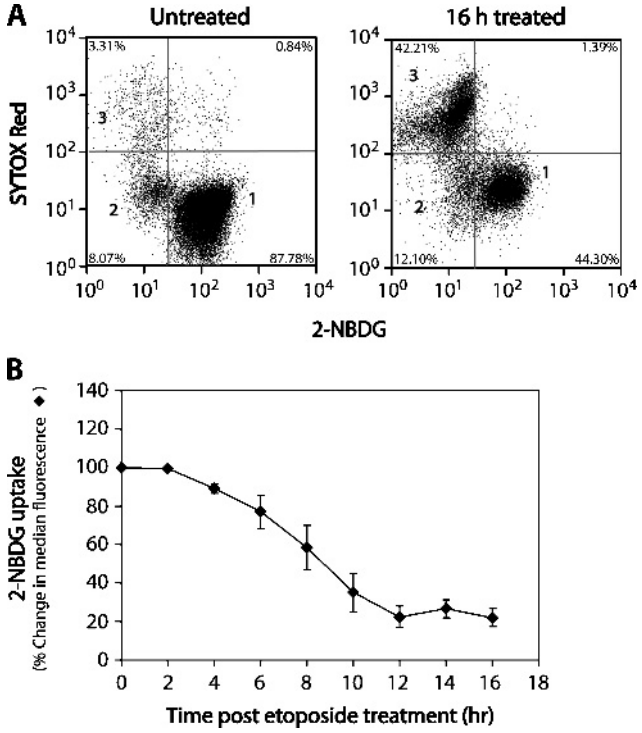


**Figure W1.** Flow cytometric analysis of 2-NBDG uptake in etoposide-treated EL-4 cells. (A) Dual-plot histogram of 2-NBDG uptake and SYTOX Red staining in 16-hour treated and untreated cells. Cells were incubated with 2-NBDG (100 $\mu$M) for 60 minutes at 37°C before the determination of uptake by flow cytometry (2-NBDG $\lambda$Ex/Em = 465/540 nm; SYTOX Red $\lambda$Ex/Em = 640/658). Population 1 represents viable cells, population 2 represents apoptotic cells, and population 3 represents necrotic cells. (B) Quantitation of 2-NBDG uptake after treatment. 2-NBDG uptake was expressed as the percentage change in median fluorescence. Mean values ($n$ = 4) and SEM are shown.

**Table W2.** Fitted Rate Constants for Untreated and Etoposide Treated Tumors.

| | $k_L$ ($s^{-1}$) | $k_P$ ($s^{-1}$) | $\rho_L = \rho_P$ ($s^{-1}$) |
|---|---|---|---|
| Untreated ($n$ = 5) | 0.018 ± 0.002 | 0.056 ± 0.005 | 0.030 ± 0.001 (34 ± 1 s) |
| Treated 16 h ($n$ = 5) | 0.023 ± 0.001 | 0.063 ± 0.006 | 0.031 ± 0.001 (32 ± 1 s) |
| Treated 24 h ($n$ = 6) | 0.022 ± 0.004 | 0.034 ± 0.006* (–38%) | 0.032 ± 0.001 (32 ± 2 s) |

Values are presented as mean ± SEM.
*$P$ < .05, ANOVA followed by Dunnett's *post hoc* test.